Ionospheric Research

NASA Grant NsG-114-61

Scientific Report

on

"An Investigation of Second-Order Corrections to First-Order Ray Theory As Applied to Beacon Satellite Transmission Studies"

by

Nevin D. Foltz

November 15, 1965

Scientific Report No. 225

Ionosphere Research Laboratory

Submitted by: W. J. Ross

W. J. Ross, Professor of Electrical Engineering

Approved by: G. N. Waynick

A. H. Waynick, Professor of Electrical Engineering
Director, Ionosphere Research Laboratory

The Pennsylvania State University

College of Engineering

Department of Electrical Engineering

Table of Contents

Abstract

13841

A review of the first-order ray theory of wave propagation through the ionosphere is presented as an introduction to the second-order ray theory. Both theories embody equations useful to the study of the total integrated electron content, N_T, of the ionosphere. Using simultaneous polarization rotation and dispersive doppler records of the Transit 4A beacon satellite recorded at Huancayo, Peru, the relative accuracy of the two theories is investigated. Results indicate that the second-order theory provides a more accurate means with which to compute N_T, and that mean ionospheric height variation with direction is a further factor which must be considered in more accurate data reduction programs.

Author

Chapter I

First-Order Ray Theory

1.1 Introduction

Since the orbiting of the first artificial earth satellite in October of 1957, many ionospheric investigators have utilized the high frequency radio transmissions from artificial earth satellites to study the total integrated electron content of the ionosphere along the signal paths. The refractive and birefringent properties of the conducting medium result in polarization rotation and phase shift effects on the satellite radio signal. These effects are cumulative along the signal path and the net result can be measured with the appropriate receiving and recording instrumentation. In the first-order ray theory, the total polarization rotation and the phase path dispersion are proportional to the total integrated electron content along the signal path.

A second-order ray theory has been developed through modification of the first-order equations to include the effects of ray refraction and mode splitting.

The purpose of this study is to compare the relative accuracy of the first and second-order ray theories with actual data received from the Transit 4A beacon satellite, and to discuss the application of the second-order theory in data reduction.

The simultaneous polarization rotation and dispersive doppler data was received at Huancayo, Peru (12.05S, 75.35W) during six passes of the Transit 4A beacon satellite from January 1962 to March 1962. The satellite radiated an elliptically polarized signal from a magnetically oriented antenna; this resulted in essentially linear polarization for an observer near the magnetic equator.

The orbital characteristics were as follows

Period 103.84 minutes

Inclination 66.8 degrees

Perigee 887 kilometers

Apogee 1007 kilometers

A description of the receiving and recording equipment used to collect the ionospheric effects can be found in references 1 and 2

1.2 Appleton-Hartree Equation and Wave Polarization

The birefringent and dispersive properties of the ionosphere for electromagnetic wave propagation affect the radio wave propagation velocity as shown by the Appleton-Hartree wave refractive index.

$$M = \left\{ 1 - \left[\frac{X}{1 - iZ - Y_L R} \right] \right\}^{\frac{1}{2}} \qquad (1\text{-}1)$$

Progressive plane electromagnetic waves exist in the ionosphere for certain values of the wave polarization R.

$$R = \frac{-i}{Y_L} \left\{ \frac{Y_T^2}{2} (1 - X - iZ)^{-1} \pm \left[\frac{Y_T^4}{4} (1 - X - iZ)^{-2} + Y_L^2 \right]^{\frac{1}{2}} \right\} \qquad (1\text{-}2)$$

The quantities appearing in (1-1) and (1-2) are defined as

$$Y_L = \frac{e|B| \cos \psi}{2\pi m f} = \frac{\omega_L}{\omega}$$

$$Y_T = Y_L \tan \psi = \frac{\omega_T}{\omega}$$

$$X = \frac{Ne^2}{4\pi^2 \epsilon_0 m f^2} = \left(\frac{\omega_N}{\omega} \right)^2$$

$Z \equiv \frac{\nu}{\omega}$

$R \equiv \frac{Ex}{Ey} = \frac{-Hy}{Hx}$

$e \equiv$ electronic charge

$m \equiv$ mass of the electron

$|B| \equiv$ magnitude of the geomagnetic field induction

$\psi \equiv$ angle between the wave normal and $\overline{B}$

$\omega \equiv$ angular wave frequency

$\omega_N \equiv$ angular plasma frequency

ω_T, $\omega_L \equiv$ angular transverse and longitudinal gyrofrequency

$N \equiv$ number density of electrons

$\nu \equiv$ collision frequency of electrons with heavy particles

$\epsilon_o \equiv$ permittivity of free space

All quantities are expressed in the rationalized MKS units.

The directions x, y, z form a orthogonal right-handed coordinate system with wave propagation in the z direction, and $\overline{B}$ lies in the y-z plane.

1.3 High Frequency Quasi-Longitudinal Propagation

For a frequency of 54 mc/s, for the angle ψ less than 88.5 degrees, and ω_N/ω sufficiently small, the equations (1-1) and (1-2) reduce to

$$n \approx \left[1 - \frac{X}{1 \pm Y_L} \right]^{\frac{1}{2}} \qquad (1\text{-}3)$$

$$R \approx \pm i$$

The quantity Z is negligible along the propagation path for beacon satellite signal frequencies.

1.4 First-Order Polarization Rotation

Assuming the quasi-longitudinal propagation conditions exist, a

linearly polarized radio wave will propagate with equal amplitudes in two modes with the wave polarization given by equation (1-4). The two circular modes propagate with different velocities, so the resultant linear polarization rotates π radians for each wavelength of phase path difference. This effect is expressed mathematically as

$$\Omega = \frac{\pi}{\lambda} \left\{ \int_+ n_+ \, d S_+ - \int_- n_- \, d S_- \right\} \text{ radians} \qquad (1\text{-}5)$$

where Ω is the total polarization rotation, λ is the propagating wavelength, and the integrals represent the phase path lengths of the two circular modes. Equation (1-5) takes on the following form when the first-order theory is assumed, which considers both modes to follow the same straight-line ray path,

$$\Omega = \frac{\pi}{\lambda} \int (n_+ - n_-) \, d S = K_1 B_L \sec \chi \, N_T \text{ radians} \qquad (1\text{-}6)$$

where $K_1 = e^3 / 8\pi^2 m^2 \epsilon_o c f^2$, $\overline{B_L \sec \chi} = \dfrac{\int B_L (\sec \chi) N \, dh}{N_T}$.

and $N_T = \int N \, dh$

The weighted mean quantities are evaluated at the mean ionospheric height or "ionospheric point". This height of this "ionospheric point" is usually assumed to be independent of satellite position for orbits of low eccentricity which lie well above the level of maximum density.

1.5 First-Order Phase Path Reduction

The motion of an orbiting beacon satellite creates an apparent frequency shift of the radio signal measured by an observer, this doppler frequency shift is a result of the phase path length changing with

satellite position. The refractivity of the ionosphere contributes to this effect, giving a change in the phase path length which is proportional to the electron content along the mode path. The time rate of change of this part of the total phase shift results in the dispersive doppler frequency shift. If the beacon satellite radiates harmonically related signals, the relative magnitude of the dispersive phase path shift can be measured with proper mixing of the received signals and the N_T along the signal path can be determined experimentally.

The number of cycles of phase path length change measured with respect to the wavelength of the higher frequency is written as

$$\Phi = \frac{\alpha}{\lambda} \left\{ \int n(\alpha f)\, dS - \int n(f)\, dS \right\} \text{cycles}, \tag{1-7}$$

αf is the higher frequency, and λ is the wavelength of the lower frequency signal. Rewriting equation (1-7) in terms of the first-order theory, we have

$$\Phi = K_2 \left(\alpha - \frac{1}{\alpha} \right) \overline{\sec \chi}\ N_T \text{ cycles} \tag{1-8}$$

where $K_2 = e^2/8\pi^2 \epsilon_o cm f$; $\overline{\sec \chi} = \dfrac{\int N \sec \chi\ dh}{N_T}$, and χ is the zenith angle of the straight line path.

1.6 Hybrid Doppler-Faraday Equations

The actual utilization of equations (1-6) and (1-8) to compute N_T requires knowledge of Φ and Ω as a function of satellite position. Let us write equations (1-6) and (1-8) as

$$\Omega = \Omega(t_i) = \Omega_{io} + \Omega_o \tag{1-9}$$

and $$\Phi = \Phi(t_i) = \Phi_{io} + \Phi_o, \tag{1-10}$$

t_i is any time, and the subscript io refers to the change in the pertinent quantity between times t_i and t_o. The quantity $\Phi(t_o) = \Phi_o$ is an unknown as is $\Omega(t_o) = \Omega_o$, except in the instance when the observer sees a quasi-transverse propagation region in the ionosphere where $\Omega(t_o)$ can be determined unambiguously. Equations have been developed by O. K. Garriott and F. deMendonca to compute Φ_o and Ω_o experimentally if simultaneous polarization rotation and dispersive doppler recordings are available.[3] Their results are

$$\Omega_o = \left\{ \frac{(\overline{B_{L_1}})(\overline{B_{L_2}}) K_3 [\Phi_{10} - \Phi_{20}] + (\overline{B_{L_1}}) \Omega_{20} - (\overline{B}_{L_2}) \Omega_{10}}{(\overline{B}_{L_2}) - (\overline{B}_{L_1})} \right\} \tag{1-11}$$

and $$\Phi_o = \left\{ \frac{(\Omega_{10} - \Omega_{20})/K_3 + (\overline{B_{L_2}}) \Phi_{20} - (\overline{B}_{L_1}) \Phi_{10}}{(\overline{B}_{L_1}) - (\overline{B}_{L_2})} \right\}, \tag{1-12}$$

$$K_3 = \frac{\alpha e}{mf(\alpha^2 - 1)} \quad \text{and} \quad (\overline{B}_{Li}) = \frac{\int B_{Li} N_i \sec(\chi_i)\, dh}{N_T} .$$

Chapter II

Second-Order Ray Theory

2.1 Second-Order Assumptions

The basis of the second-order ray theory lies in the following list of assumptions concerning the wave refractive index, the medium and the "ionospheric point";

(1) Terms of degree three in (X, Y) are included in the refractive index expansion,

(2) Non-uniform ionization distribution is considered,

(3) Mode path separation is included,

(4) "Ionospheric point" height depends on the satellite zenith angle.

The first three assumptions were included in an extension to the first-order equations by W. J. Ross.[4]

2.2 Second-Order Polarization Rotation

An equivalent first-order polarization rotation angle $\omega(t_i)$ which is corrected for the second-order effects is related to the total polarization $\Omega(t_i)$ observed at the receiver as

$$\omega(t_i) = \frac{\Omega(t_i)}{\left[1 + \frac{\beta \bar{X}}{2} + \frac{(\beta - 1) G \bar{X}}{2}\right]} \text{ radians.} \qquad (2\text{-}1)$$

β is a distribution parameter representing the non-uniformity of ionization along the first-order ray path, and is defined by $\beta = \overline{X^2} / \bar{X}^2$ An approximate value for β can be computed using a plane Chapman model of the ionosphere; results of such computations are shown in Table I. In Table I, h_o is the height of the maximum ionization density while H_1 and H_2 are the scale heights below and above h_o respectively.

TABLE 1

DISTRIBUTION FUNCTION - β

	β	h_c(km)	H_1 (km)	H_2(km)
1.	2.01	250	50	100
2.	2.10	350	50	100
3.	2.25	250	40	80
4.	2.36	300	40	80
5.	2.27	250	50	80
6.	2.33	300	50	80
7.	1.96	250	40	100
8.	2.02	300	40	100
9.	2.50	250	67	67

β is most sensitive to changes in H_2 since most of the ionization lies above h_2; reasonable changes in H_1 and h_o effect relatively small changes in β.

The geometrical parameter G is a function of the angle θ between the first-order ray path and the local vertical to the plane of uniform ionization at the "ionospheric point", and the angle η between the first-order ray path and the magnetic field component in the plane of incidence at the "ionospheric point". The parameter $G = \tan\theta \left[\tan\theta - \tan\eta \right]$ compensates for wave-normal refraction and ray-wave normal-separation effects. A map showing the value of G for an observer at (12.05 S, 75.35 W) as a function of satellite longitude and latitude, is shown in Figure 1.

2.3 Second-Order Phase Path Dispersion

The total number of cycles phase path length change, for a radio signal from the satellite to the observer, referred to the higher frequency can be expressed in the second order theory as

$$\phi(t_1) = \frac{\Phi(t_1)}{\left[1 \mp Y_L + \frac{\beta \bar{X}}{4} + (\beta - 1)\bar{X}\tan^2\theta\right]} \text{ cycles,} \qquad (2\text{-}2)$$

where $\Phi(t_1)$ is the quantity measured at the receiver, and $\phi(t_1)$ is the equivalent first-order value corrected for the second-order effects.

It has been shown through a model study that use of the mode corresponding to the positive sign for Y_L will reduce the effect of the second-order correction factor.[4] When equations (2-1) and (2-2) are utilized in data reduction, one must remember that the equations are true only for high frequency, quasi-longitudinal propagation conditions.

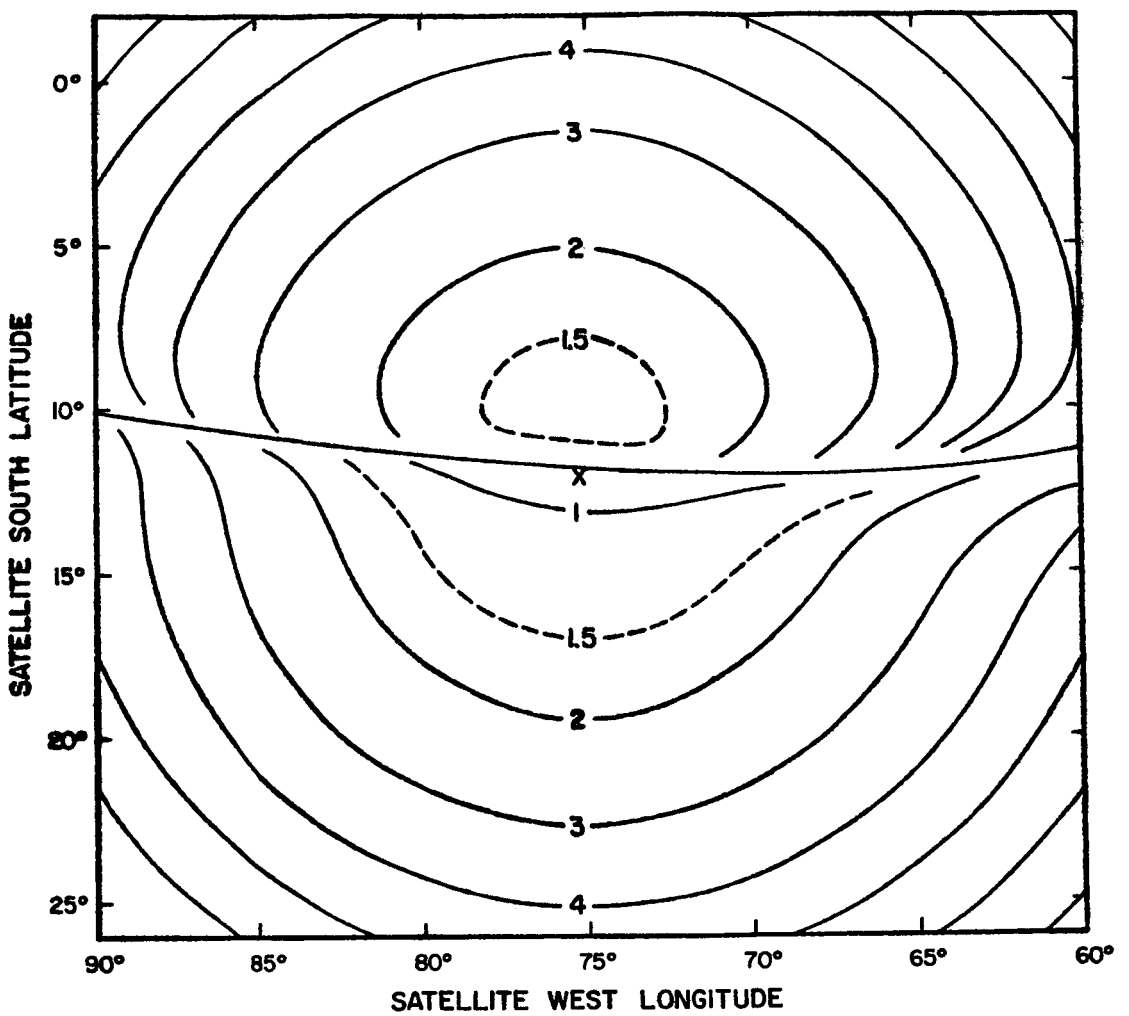

CONTOUR MAP OF THE PARAMETER G
FOR HUANCAYO , PERU X
SATELLITE HEIGHT 1000 KM , IONOSPHERE HEIGHT 400 KM

FIGURE .

2.4 Second-Order Hybrid Equation

The second-order quantities ω_o and ϕ_o, completely analogous to those of the first-order theory, can be determined as follows

$$\omega_o = \left\{ \frac{(\bar{B}_{L_1})(\bar{B}_{L_2}) K [\phi_{10} - \phi_{20}] + \bar{B}_{L_1}) \omega_{20} - (\bar{B}_{L_2}) \omega_{10}}{(\bar{B}_{L_2} - \bar{B}_{L_1})} \right\} \text{radians}, \tag{2-3}$$

and $$\phi_o = \frac{[(\omega_1 - \omega_2)/K_3 + (B_{L_2}) \phi_{20} - (B_{L_1}) \phi_{10}]}{(B_{L_1} - B_{L_2})} \text{ cycles}. \tag{2-4}$$

We can also write

$$\omega(t_i) = \omega_{io} + \omega_o \tag{2-5}$$

and $$\phi(t_i) = \phi_{io} + \phi_o. \tag{2-6}$$

2.5 Height Variation of the "Ionospheric Point" with Satellite Zenith Angle

The second-order theory also considers the effect of the "ionospheric point" height on the relative satellite and observer positions.

A model was constructed to study the variation of the "ionospheric point" height with satellite zenith angle. The model consisted of a spherical earth containing a centered dipole magnetic field with the magnetic pole at (78.6 N, 75.35 W). The satellite was assumed to pass over observers at (40.79N, 77.86 W) and (12.05 S, 75.35 W) in a magnetic meridian plane. Two models of ionization density profiles were considered; in Case 1 the ionization density profile consisted of three parabolic curves connected to approximate an actual daytime ionosphere, and in case two the ionization lay in a uniform plane layer.

$$\text{In case one,} \quad N(r) = N_o (C_{1_i} + C_{2_i} r + C_{3_i} r^2) \tag{2-7}$$

where i corresponds to a specific range of r measured from the center of the earth, and the constants C_{ji} (j = 1, 2, 3) are determined by the boundary conditions at the parabola intersections. In case two, $N(r) = N_o$ for $r_1 \leq r \leq r_2$ and zero for all other values of r. With each model of the ionosphere, a closed form expression of $\overline{B_L \sec \chi}$ as a function of the relative satellite and observer positions, was found and the "ionospheric point" height was obtained.

The expression for a dipole magnetic field is

$$\bar{B} = B_o \left(\frac{r_o^3}{r}\right) \left[2 \cos\theta \, \hat{r} + \sin\theta \, \hat{\theta}\right], \tag{2-8}$$

where r_o is the radius of the earth, and B_o is the magnitude of $\bar{B}$ at $r = r_o$ and $\theta = \pi/2$ radians.

The unit vector lying along the straight line signal path can be written as $\bar{n} = (\bar{r}_s - \bar{r}_o) / |\bar{r}_s - \bar{r}_o|$, where $\bar{r}_o$ and $\bar{r}_s$ are the position vectors of the observer and satellite respectively.

2.6 Model Computation of $\overline{B_L \sec \chi}$

The weighted mean of $B_L \sec \chi$ can be written as

$$\overline{B_L \sec \chi} = \frac{\int \bar{B} \cdot \bar{n} \, N(r) \sec \chi(r) \, dr}{\int N \, dr}, \tag{2-9}$$

with integration being taken along the first-order ray path, (i.e. the straight line) from satellite to observer. The factors in the integrand can be defined as

$$\bar{B} \cdot \bar{n} = \frac{2 B_o r_o^3 \sin\alpha}{r} \left\{1 - \frac{3\gamma^2}{2r^2} + \frac{3\gamma \cot\alpha}{2r} \sqrt{1 - \frac{\gamma^2}{r^2}}\right\}, \tag{2-10}$$

with $\gamma = r_o \sin(\theta_s - \theta_o) / \left[1 + \left(\frac{r_o}{r_s}\right)^2 - 2 \frac{r_o}{r_s} \cos(\theta_s - \theta_o) \right]^{\frac{1}{2}}$,

$$\sin \alpha = \gamma \left[\frac{\cos \theta_s - (r_o/r_s)\cos \theta_o}{r_o \sin(\theta_s - \theta_o)} \right], \text{ and } \sec \chi = \left[1 - \frac{\gamma^2}{r^2} \right]^{-\frac{1}{2}},$$

θ_s and θ_o are the colatitudes of the satellite and observer respectively. When N(r) takes the form of Case 1, integration must be carried out between three sets of limits corresponding to i = 1, 2, 3 for the constants C_{ji}. The result of carrying out the integration in equation (2-8) with N(r) defined by case one is

$$\overline{B_L \sec \chi} = \frac{2B_o r_o^3 N_o \sin \alpha}{N_T} \left\{ C_{3i} \left[\ln r + \ln \left(1 + \sqrt{1 - \gamma^2/r^2}\right) \right] + \frac{C_{2i}}{4|\gamma|} \cos^{-1} \left| \frac{\gamma}{r} \right| \right.$$

$$\left. - \left[\frac{C_{1i}}{3r^2} + \frac{C_{2i}}{2r} + C_{3i} \right] \left[\frac{3 \cot \alpha}{2} \left(\frac{\gamma}{r} \right) + \frac{3}{2} \sqrt{1 - \gamma^2/r^2} \right] \right\} \Bigg|_{r_1}^{r_2} \quad i=1 \qquad \Bigg|_{r_2}^{r_3} \quad i=2 \qquad \Bigg|_{r_3}^{r_4} \quad i=3, \tag{2-11}$$

this quantity $\overline{B_L \sec \chi}$ is now a function of θ_s and θ_o.

A similar result for N(r) as in case (2) is

$$\overline{B_L \sec \chi} = B_o r_o^3 \left\{ \frac{\sqrt{1 - \gamma^2/r^2} \sin \alpha + \left(\frac{\gamma}{r}\right) \cos \alpha}{r^2 (r_1 - r_2)} \right\} \Bigg|_{r_2}^{r_1}, \tag{2-12}$$

The centered dipole magnetic field was chosen for two reasons, it is a good representation of the geomagnetic field in the equatorial latitudes, and it resulted in a closed form expression for $\overline{B_L \sec \chi}$. This magnetic field model was also used for the observer at (40.79°N, 77.86°W), however

it was shown by O. K. Garriott and F. deMendonca that the dipole magnetic field for an observer at mid-latitudes, is within ten per cent of a spherical harmonic expansion of the geomagnetic field for satellite latitudes about six degrees to the North and South of the observer.[5] Figures 2 and 3 show the variation of $B_L \sec \chi$ along the first-order ray path as a function of altitude. All angular coordinates are geographic, measured from the North pole.

Figure 3 reflects the symmetrical magnetic field existing about the magnetic equator and the quasi-transverse propagation region where $B_L \sec \chi$ is zero. In Figure 2 there is evidence of an approaching quasi-transverse propagation condition for a satellite to the North of θ_o, and also of more variation in $B_L \sec \chi$ versus altitude when the satellite zenith angle becomes large, so that the lower regions of the ionosphere will experience greater weighting in equation (2-8), this in effect will lower the height of the "ionospheric point" in this and similar ionospheric regions.

The height of the "ionospheric point" was also computed as a function of satellite colatitude for observers at the colatitudes θ_o indicated in Figures 2 and 3, these results are shown in Figure 4 and 5. Figure 5 represents $\bar{r}$ versus satellite colatitude to the North of θ_o only, this is a result of the magnetic field symmetry existing for this observer. It is quite evident from the curve that the variation of $\bar{r}$ does depend on satellite colatitude in this model study and this phenomenon should be considered as a second-order effect which could be absorbed into a data reduction program. Figure 4 represents a similar situation for the observer in mid-latitudes, the sharper decrease in $\bar{r}$ occurs to the North of the observer since the weighting there is greatest in the "tail" of the ionization profile as seen in Figure 2. Similar computations of $\bar{r}$ for

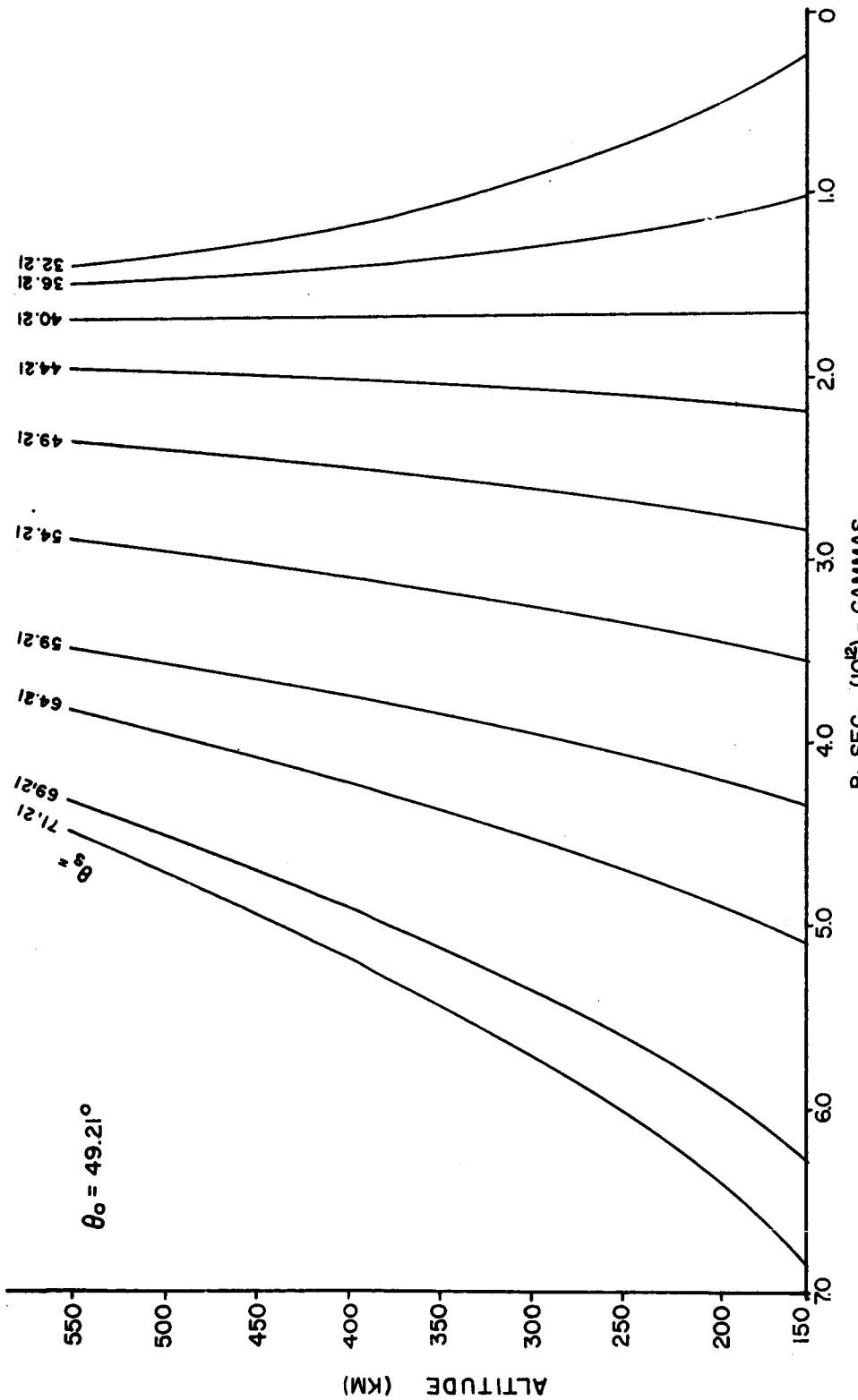

BL SEC χ VS. ALTITUDE WITH θ_s AS A PARAMETER

FIGURE 2

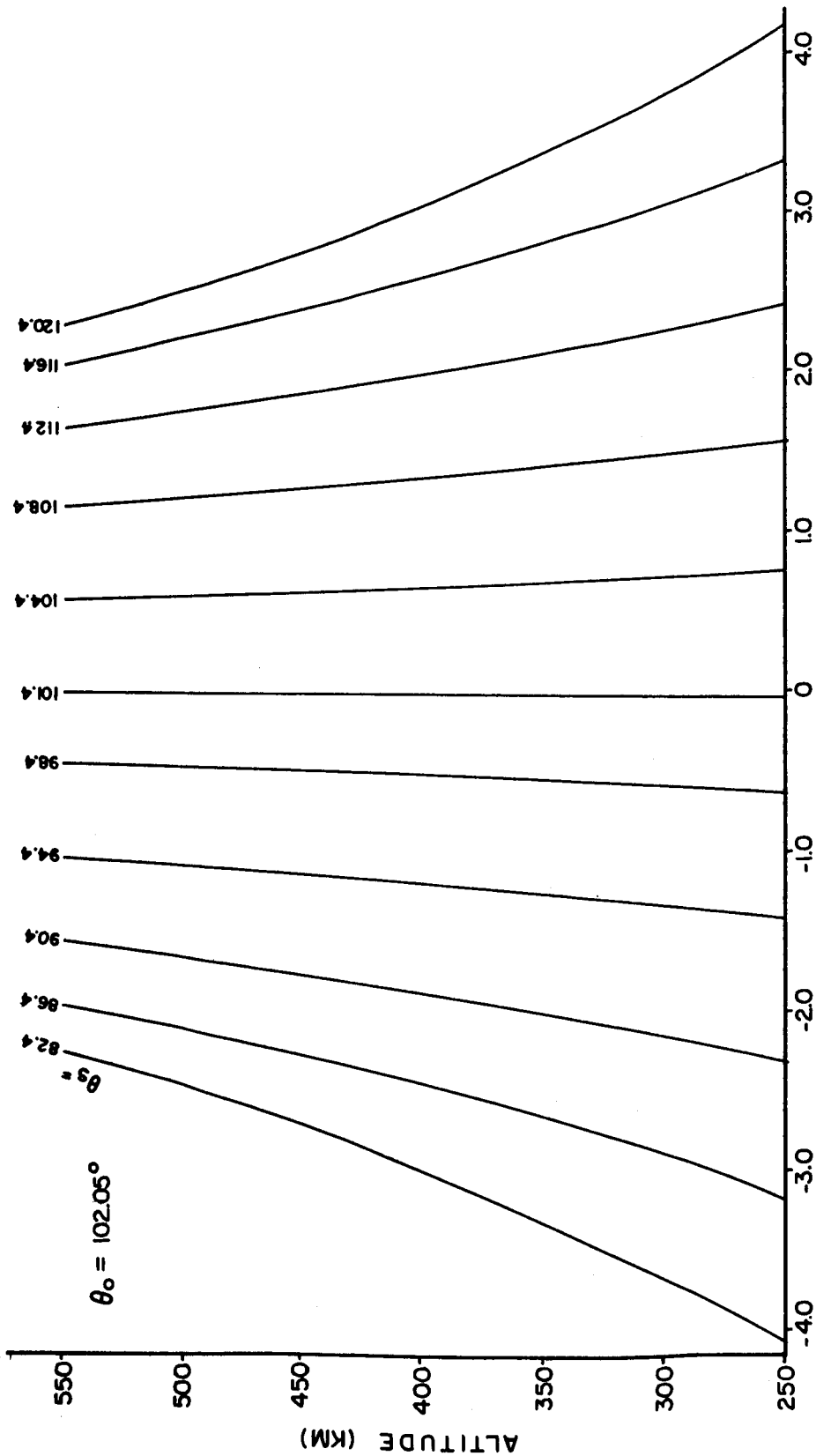

$B_L \sec\chi$ VS. ALTITUDE WITH θ_s AS A PARAMETER

FIGURE 3

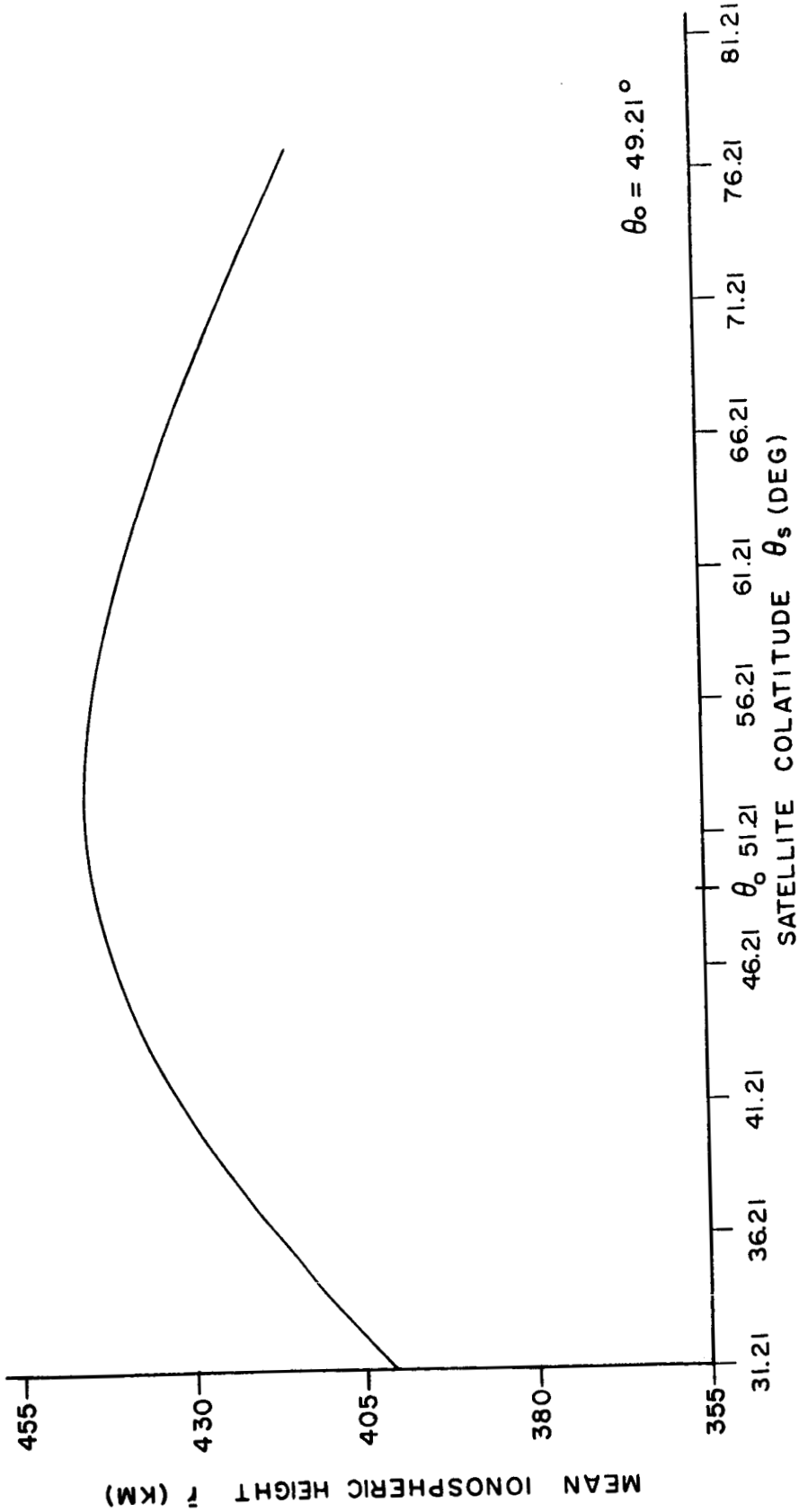

MEAN IONOSPHERE HEIGHT VS SATELLITE COLATITUDE

FIGURE 4

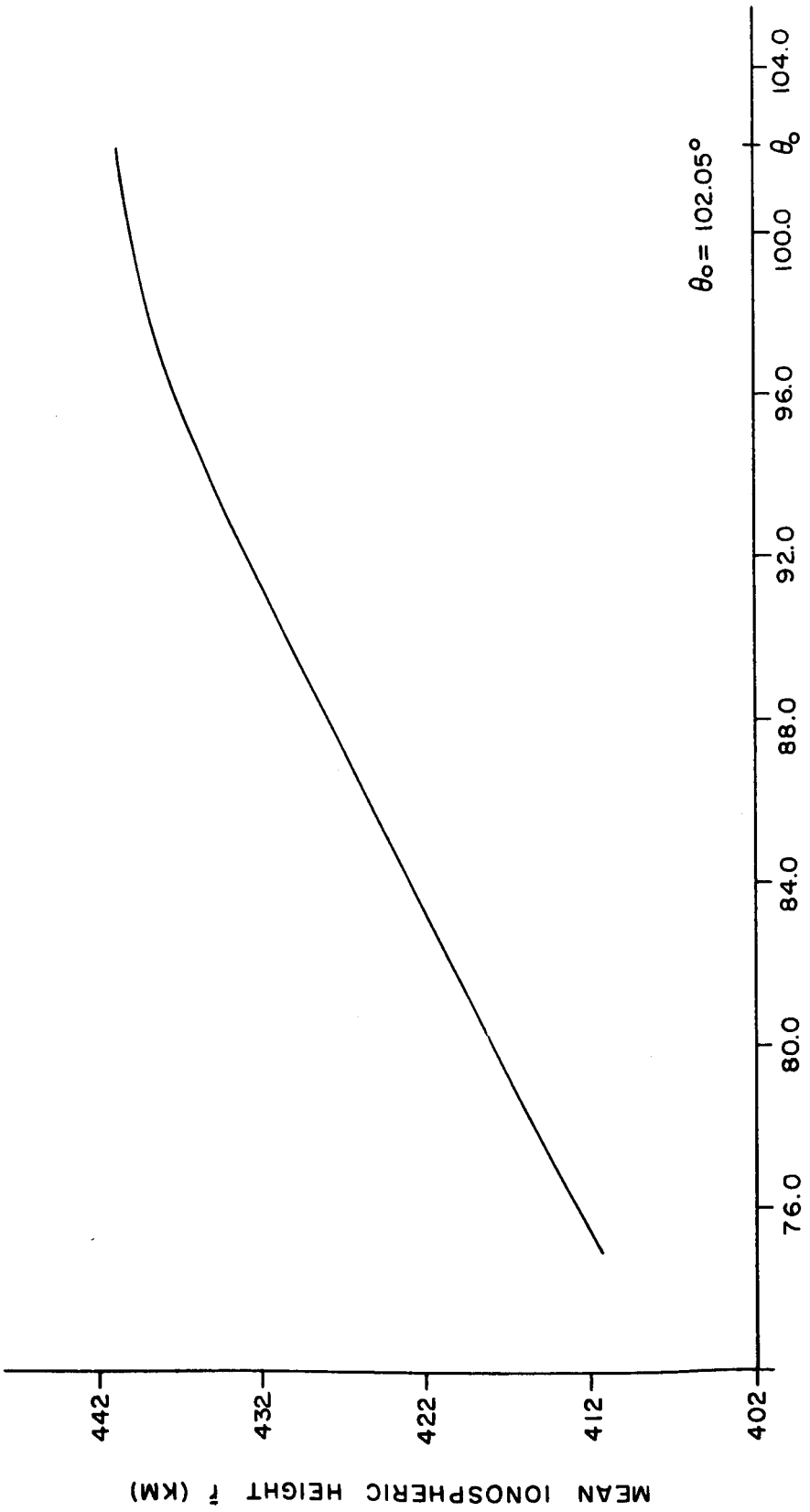

MEAN IONOSPHERIC HEIGHT VS SATELLITE COLATITUDE

FIGURE 5

Case 2 show a relatively small variation in $\bar{r}$, however the decrease in $\bar{r}$ with satellite zenith angle does increase when the layers of ionization are lower in the ionosphere, emphasizing the increased effect of B_L sec χ as $\bar{r}$ decreases. From these results, $\bar{r}$ can be assumed to follow first-order theory for a nighttime ionosphere when the ionization is more confined to a relatively thin layer.

Chapter III

Data Reduction Methods

3.1 Introduction

Simultaneous polarization rotation and dispersive doppler data were recorded by a station at Huancayo, Peru (12.05 S, 75.35 W) from six passes of the Transit 4A beacon satellite. Satellite passage information is listed in Table 2.

3.2 Quasi-Transverse Propagation

A unique propagation condition exists for observers located near the magnetic equator. In this region, mode paths exist for which the propagation is quasi-transver, for a propagation frequency of 54 Mc/sec., i.e. ψ is greater than 88.5 degrees. For a satellite at 1000 kilometers altitude, this propagation condition exists for about three seconds of the satellite pass. I can be shown that the quasi-longitudinal regions on either side of the quasi-transverse region may be connected with a linear interpolation of the first-order equation. With knowledge of the quasi-transverse region, $\Omega(t_i)$ and hence $\omega(t_i)$ can be measured unambiguously.

3.3 Application of the Hybrid Doppler-Faraday Equations

The hybrid Doppler-Faraday equations (1-11) and (1-12) provide a method to determine Φ_o and Ω_o when simultaneous polarization rotation and dispersive doppler data is available. These equations can also be used to compare the relative accuracy of the first and second order ray theory. Since Ω_o and Φ_o are theoretical constants for each satellite pass, a plot of either of these quantities and the associated second-order quantity ω_o or ϕ_o versus certain values of t_i, provides a comparison of the relative accuracy in the first and second-order theories.

TABLE 2

SATELLITE PASSAGE INFORMATION

	Date	Time	Direction	N_T (electrons/m^2)
1.	1-20-62	12:42:23 to 12:35:25	S to N	2.833×10^{17}
2.	3-7-62	15:24:58.6 to 15:31:14.6	N to S	4.176×10^{17}
3.	3-10-62	14:21:58.4 to 14:27:52.0	N to S	3.321×10^{17}
4.	3-14-62	13:31:56.4 to 13:38:50.0	N to S	3.983×10^{17}
5.	3-18-62	12:43:31.0 to 12:49:47.0	N to S	4.354×10^{17}
6.	3-26-62	11:05:23.0 to 11:11:41.0	N to S	4.137×10^{17}

The quantity $\Omega(t_i)$ is known unambiguously for the observer at Huancayo, Peru, so as a matter of completeness Φ_o and ϕ_o were chosen for the comparison.

Each computation of equation (1-12) requires a choice of times t_o, t_1, t_2. The time t_o was chosen to be approximately the time of quasi-transverse propagation and hence the satellite would be nearly overhead, the times t_1 and t_2 were chosen to be nearly symmetrical about t_o. If the times t_1 and t_2 are chosen as mentioned above, then propagation conditions along the two first-order ray paths are likely to be similar. This similarity in propagation conditions reduces the possibility of introducing any unnecessary weighting in the equations for Φ_o and ϕ_o, and provides nearly equal satellite zenith angles for both times t_1 and t_2.

All terms in equation (1-12) were obtained experimentally except $\overline{B_{Li}}$ which was computed as a function of t_i, using a spherical harmonic expansion employing Jensen and Cain coefficients for Epoch 1960 for the magnetic field. The "ionospheric point" was taken to lie at an altitude of 400 kilometers, nearly the altitude of the maximum ionization density for a daytime ionosphere. The satellite passes listed in Table 2 provided propagation conditions which enhanced the second-order parameters, such as maximum integrated electron density, and had also clear, continuous signal strength at time t_i corresponding to large satellite zenith angles.

The actual value of Φ_o and ϕ_o used in equations (1-10) and (2-6) to compute N_T for each satellite pass, is an average of the quantities which are computed for a number of times t_i on either side of t_o.

Chapter IV

Comparison of First and Second Order Results

4.1 Introduction

The quantities Φ_o and ϕ_o were computed of a function of t_1 and t_2 for the satellite passages in Table 2. The times t_1 and t_2 were chosen as described in Section 3.3 For a number of the satellite passes a variation in the ionospheric point as dictated by Section 2.5 of this report was included in the computations for ϕ_o.

4.2 Discussion of Results

The plots of Φ_o and ϕ_o versus satellite colatitude, measured in degrees on either side of the observer, appear in Figures 6(a)-6(f). Each plot corresponds to one satellite pass.

The most noticeable effect of the second-order theory is a decrease in Φ_o to ϕ_o which is more pronounced as $|t_o - t_i|$ increases. This overall decrease Φ_o is evident from equation (2-2) where ϕ_o is a fraction of Φ_o dependent on the magnitude of the second-order correction terms. At increasing zenith angles the radio signal passes through proportionately more ionization at lower heights; this effect can lower the height of the ionospheric point at large zenith angles. In computing Φ_o and ϕ_o the ionospheric point was assumed to lie at a constant altitude, so that a decrease in this altitude would remove some of the remaining slope in the ϕ_o curve at the 5, 6, 7, and 8 degree points. In general the ϕ_o curve is flatter between the 3 to 6 degree points, than the Φ_o curve which is a trend toward the theoretical constancy. Any ϕ_o curves which have a negative slope in the 3 to 6 degree region of the curve could be attributed to an erroneous

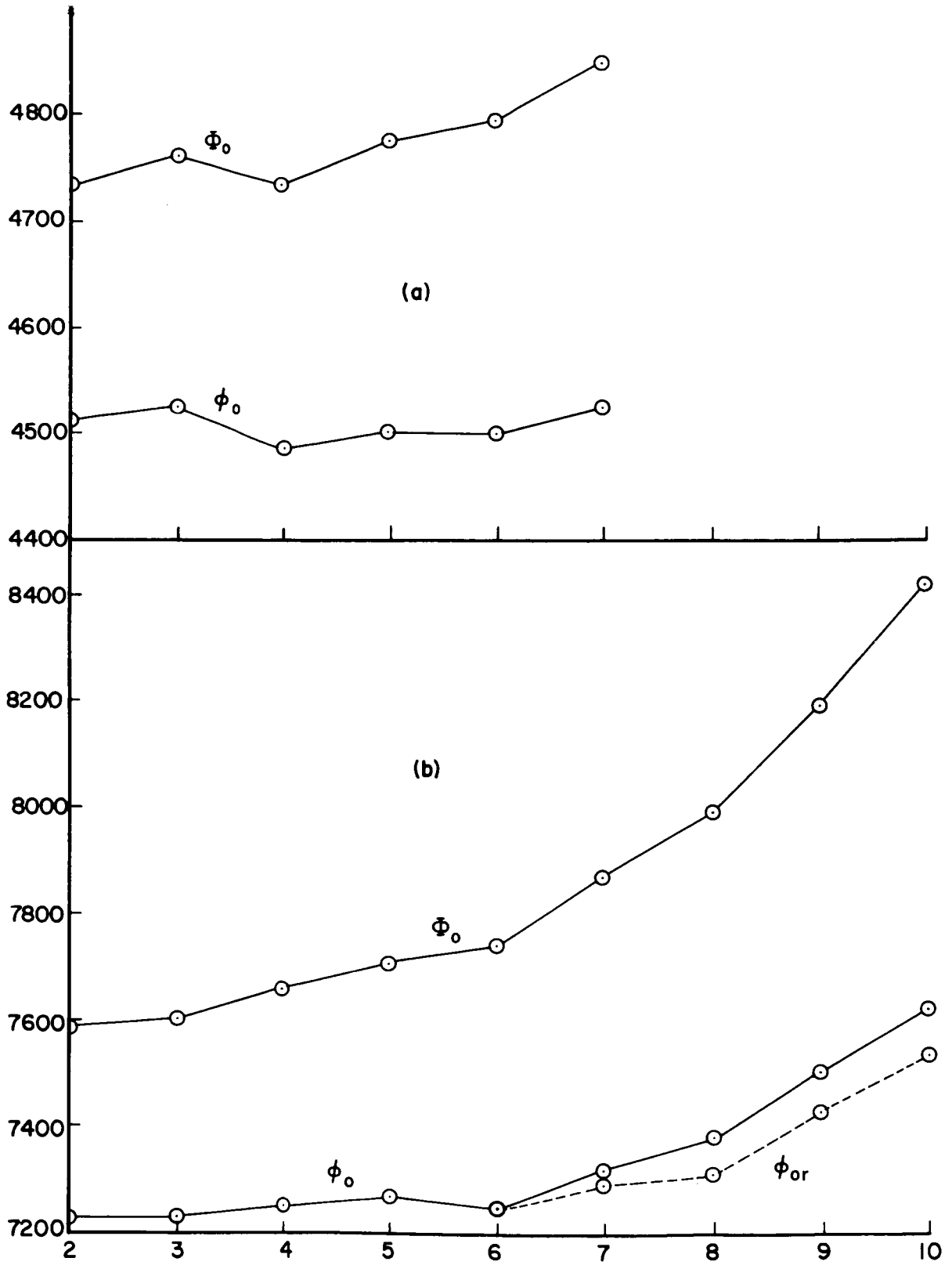

MAGNETIC LATITUDE OF SATELLITE

FIGURES 6a, 6b

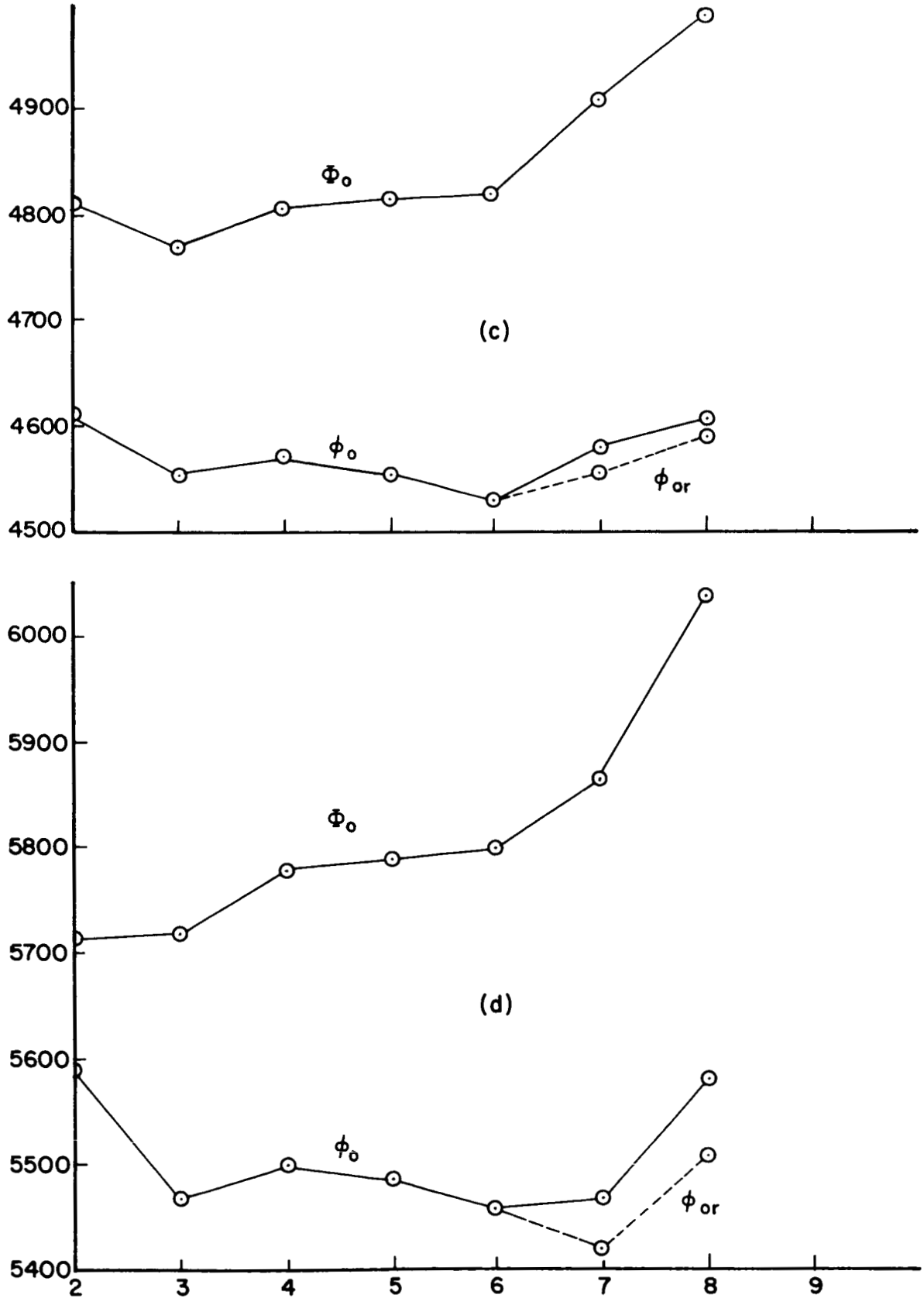
4900
4800
4700
4600
4500
Φ_o
(c)
ϕ_o
ϕ_{or}
6000
5900
5800
5700
5600
5500
5400
Φ_o
(d)
ϕ_o
ϕ_{or}
2
3
4
5
6
7
8
9
MAGNETIC LATITUDE OF SATELLITE

FIGURE 6c, 6d

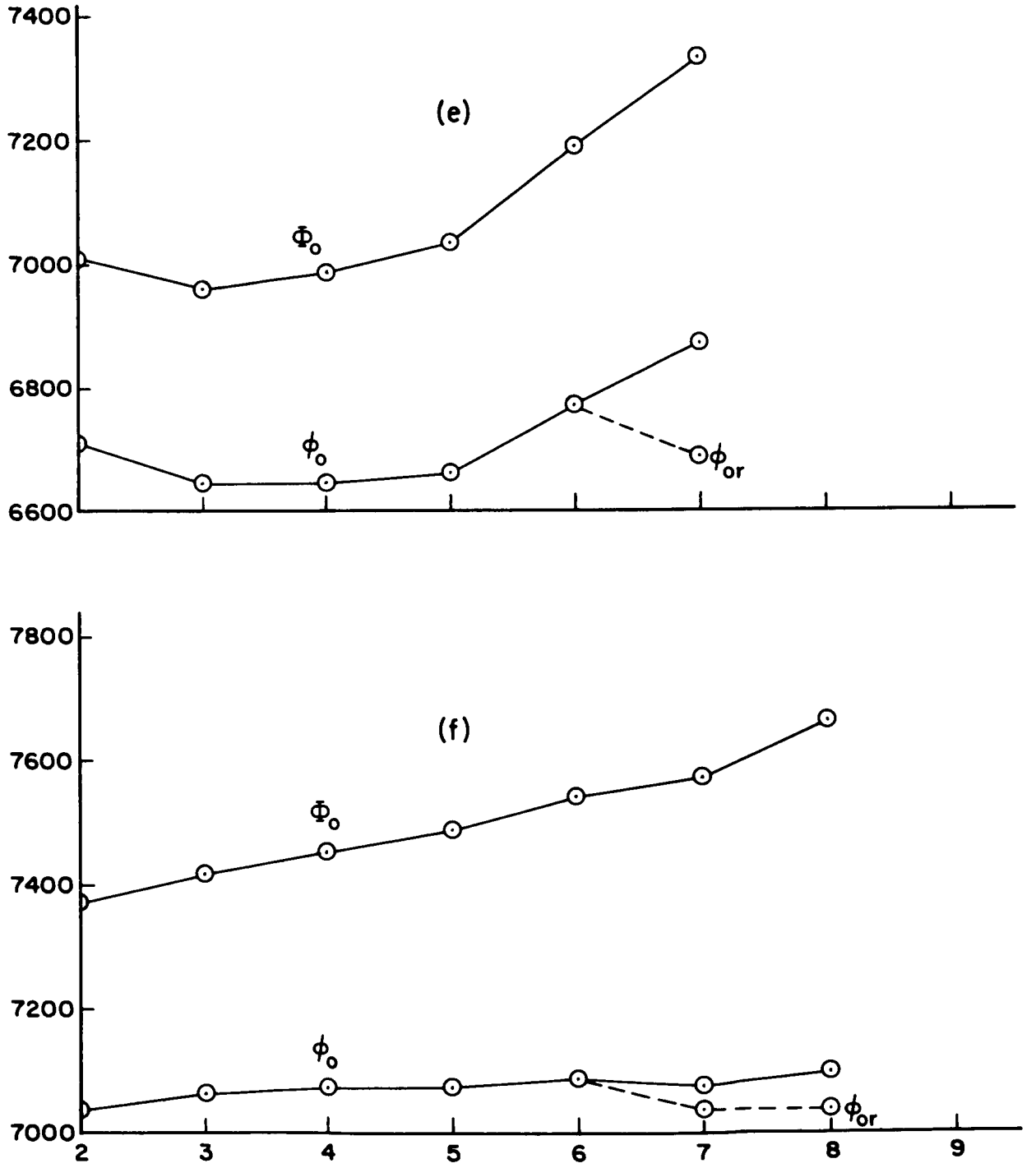
7400
7200
7000
6800
6600
(e)
Φ_o
ϕ_o
ϕ_{or}
7800
7600
7400
7200
7000
(f)
Φ_o
ϕ_o
ϕ_{or}
2
3
4
5
6
7
8
9
MAGNETIC LATITUDE OF SATELLITE

FIGURE 6e, 6f

choice of the ionospheric point altitude.

The erratic behavior of both curves in the 2 and 3 degree region is most likely related to the sensitivity of the recorded data and to reduction errors, and computations in this region of the curve will be least reliable.

For a number of satellite passes a decrease in $\bar{r}$ as dictated from a model study, Section (2-5), was included in the computation of ϕ_o for data points at 6, 7, and 8 degrees. These values of ϕ_o represented by the dashed curves. In most cases the dashed curve further approaches the theoretically constant value, however in Figure 6c and 6d the dashed curve only makes the curve of ϕ_o erratic. For these passes the $\bar{r}$ was evidently in error. The remaining positive slope of the ϕ_o curve could be attributed to an actual ionosphere much different from the model, or an inadequacy of the second-order theory at large satellite zenith angles. The actual variation in $\bar{r}$ used in data reduction will depend to some extent on the original value of $\bar{r}$, the satellite ephemeris, and the time of day.

Chapter V

Improved Method of Data Reduction

5.1 Introduction

From the results of Chapter IV, the second-order theory provides a higher degree of consistency in the total polarization rotation and phase path dispersion data necessary to compute the total integrated electron content, than that available in first-order theory for a daytime ionosphere.

Actual computation of N_T using the second order equations requires knowledge of the second order parameters and ionospheric point altitude as a function of satellite position. The accuracy of the results will depend greatly on the variation of $\overline{r}$ with satellite zenith angle.

5.2 Variation of $\overline{r}$ with Satellite Zenith Angle

The value of $\overline{r}$ for satellite positions corresponding to small zenith angles can be computed from a local electron density profile. In general, if the choice of $\overline{r}$ is too low, the Φ_o curve will show a less positive gradient and the ϕ_o curve will experience a negative gradient at relatively small satellite zenith angles. An acceptable value of $\overline{r}$ can be chosen without much difficulty for small values of the angle χ so that ϕ_o is constant.

The actual decrease in $\overline{r}$ for larger values of χ must be computed for each satellite position as the zenith angle increases. A first-order computation will give an approximate value for the variation in $\overline{r}$. For the observer on the equator, choose times t_i on both sides of t_o such that $\overline{B_{Li}}$ for both values of t_i are numerically equal, then equation (1-12) becomes

$$\Phi_o = \frac{K_3 (\Omega_1 - \Omega_{20}) - \overline{B_L}_{10} (\Phi_{20} + \Phi_{10})}{2\overline{B_{L_1}}} \tag{5-1}$$

Now compute Φ_o again with a new set of times t_3 and t_4 such that $\left| t_o - t_3 \right| > \left| t_o - t_1 \right|$, then we have

$$\Phi_o = \frac{K_3 (\Omega_{30} - \Omega_{40}) - \overline{B_{L_3}} (\Phi_{40} + \Phi_{30})}{2\overline{B_{L_3}}} \tag{5-2}$$

If t_1 and t_2 correspond to satellite positions where $\bar{r}$ has not changed appreciably from the small zenith angle value, then an approximate decrease in $\bar{r}$ for time t_3 and t_4 can be computed as follows; equate equations (5-1) and (5-2) and solve for $\overline{B_{L_3}}$. With appropriate magnetic field maps $\bar{r}_3$ and $\bar{r}_4$ can be found to first-order, these values of $\bar{r}$ can now be used in the computation of N_T. This procedure can be repeated for as many data points as is necessary.

5.3 Effect of Satellite Rotation

Another factor which could affect the magnitude of Φ_o and hence ϕ_o, is satellite rotation related to the quantity $\Omega(t_i)$. This effect is present when the satellite rotation vector has a component parallel to the first-order ray path.

For the Transit 4A satellite the antenna is mounted transverse to the magnetic axis, and rotation can take place only about this axis. If the antenna is truly orthogonal to the axis and the field, then an observer will see the sense of rotation reverse through the transverse point. Since the Faraday rotation is continuous in direction, the effect would be to produce an apparent discontinuity in the electron content at

the equator.

For analyses as above which bracket the equator symmetrically, the rotation difference, $\Omega_{10} - \Omega_{20}$, is essentially unaffected.

When the initial polarization is not orthogonal to the axis the discontinuity will generally appear away from the equator and a net effect in $\Omega_{10} - \Omega_{20}$ may be expected, which will lead to non-constant values of ϕ_o over the field of view.

The satellite rotation was internally damped, and was designed not to exceed about 0.001 rotations/second. This might conceivably lead to errors of the order of one percent for daylight Faraday records, and could be rather more serious at night when the ionospheric Faraday rotation is much smaller.

Chapter VI

Summary and Conclusions

It has been shown by the analysis of doppler dispersion and Faraday rotation data taken simultaneously from an equatorial station, that the use of second-order equations for the reduction of these data to electron content results in a greatly improved consistency.

Two additional considerations have been examined. In the first a model study has been made of the variation of the mean ionospheric height which is appropriate in the Faraday effect equations, as a function of satellite position. This effect, which takes into account the changed weighting given to different height ranges as the zenith angle of the source is varied, has been shown to further improve the self consistency of the analyses. As a corollary to this effect, it is evident that variation in the height of the ionospheric layers with geographic position should be included where feasible in second order analyses, especially for those made at low latitudes.

ACKNOWLEDGEMENTS

The guidance received from Dr. W. J. Ross is greatly appreciated. The work of the computing staff of the Laboratory is gratefully acknowledged.

The geomagnetic field computations were procured by Mr. Leo J. Blumle of the Goddard Space Flight Center. The orbital ephemeris was obtained from the Applied Physics Laboratory, John Hopkins University.

The recording facility at Huancayo, Peru was operated in cooperation with the Instituto de Geofisico del Peru.

This work was supported by the National Aeronautics and Space Administration under Grant NsG-114-61.

BIBLIOGRAPHY

1. Chisholm, G.E., "Observations of Large Scale Ionospheric Irregularities as Deduced from Satellite Information" Scientific Report No. 166, Ionosphere Research Laboratory, Pennsylvania State University.

2. Butler, H. W., "An Investigation of Horizontal Gradients in the Electron Content of the Ionosphere" Scientific Report No. 165, Ionosphere Research Laboratory, Pennsylvania State University.

3. Garriott and deMendonca, Ionospheric Electron Content Calculated by a Hybrid Faraday-Doppler Technique, Journal of Atmospheric and Terrestrial Physics, 24, 317-321 (1962).

4. Ross, W. J., Second-Order Effects in High Frequency Transionospheric Propagation, Journal of Geophysical Research, Vol. 70, No. 3, February 1, 1965.

5. Yeh, K. C. and Gonzalez, Note on the Geometry of the Earth's Magnetic Field Useful to Faraday Effect Experiments, Journal of Geophysical Research, 65, 3209-3214 (1960).